Journal of
Mechanics of
Materials and Structures

MICROSTRUCTURE-BASED MODELING OF ELASTIC FUNCTIONALLY GRADED MATERIALS: ONE-DIMENSIONAL CASE

Zahra Sharif-Khodaei and Jan Zeman

Volume 3, № 9 November 2008

mathematical sciences publishers

JOURNAL OF MECHANICS OF MATERIALS AND STRUCTURES
Vol. 3, No. 9, 2008

MICROSTRUCTURE-BASED MODELING OF ELASTIC FUNCTIONALLY GRADED MATERIALS: ONE-DIMENSIONAL CASE

ZAHRA SHARIF-KHODAEI AND JAN ZEMAN

Functionally graded materials (FGMs) are two-phase composites with continuously changing microstructure adapted to performance requirements. Traditionally, the overall behavior of FGMs has been determined using local averaging techniques or a given smooth variation of material properties. Although these models are computationally efficient, their validity and accuracy remain questionable, since a link with the underlying microstructure (including its randomness) is not clear. In this paper, we propose a numerical modeling strategy for the linear elastic analysis of FGMs systematically based on a realistic microstructural model. The overall response of FGMs is addressed in the framework of stochastic Hashin–Shtrikman variational principles. To allow for the analysis of finite bodies, recently introduced discretization schemes based on the finite element method and the boundary element method are employed to obtain statistics of local fields. Representative numerical examples are presented to compare the performance and limitations of both schemes. To gain insight into similarities and differences between these methods and to minimize technicalities, the analysis is performed in the one-dimensional setting.

1. Introduction

Generally speaking, the ultimate goal of every design is a product which fully utilizes the properties of the materials used in its construction. This philosophy, in the larger context, naturally leads to the appearance of multiphase composites with microstructure adapted to operation conditions [Petrtýl et al. 1996; Bendsøe and Sigmund 2004; Ray et al. 2005]. Functionally graded materials (FGMs) present one important man-made class of such material systems. Since their introduction in 1984 in Japan as barrier materials for high-temperature components, FGMs have proved to be an attractive choice for numerous applications such as wear resistant coatings, optical fibers, electrical razor blades and biomedical tools [Neubrand and Rodel 1997; Uemura 2003]. To provide a concrete example, consider a microstructure of Al_2O_3/Y-ZrO_2 ceramics (see Figure 1) engineered for the production of all-ceramic hip bearings. In this case, controlled composition and porosity allow us to achieve better long-term performance and hence lower clinical risks when compared to traditional metallic materials [Anné et al. 2006].

As typical of all composites, the analysis of FGMs is complicated by the fact that the explicit discrete modeling of the material microstructure results in a problem which is intractable due to its huge number of degrees of freedom (DOFs) and/or its intrinsic randomness. Models with given smoothly varying material data are often employed as the most straightforward answer to this obstacle. When the spatial nonhomogeneity is assumed to follow a sufficiently simple form, this premise opens the route to very

Keywords: functionally graded materials, statistically nonuniform composites, microstructural model of fully penetrable spheres, Hashin–Shtrikman variational principles, finite element method, boundary element method.

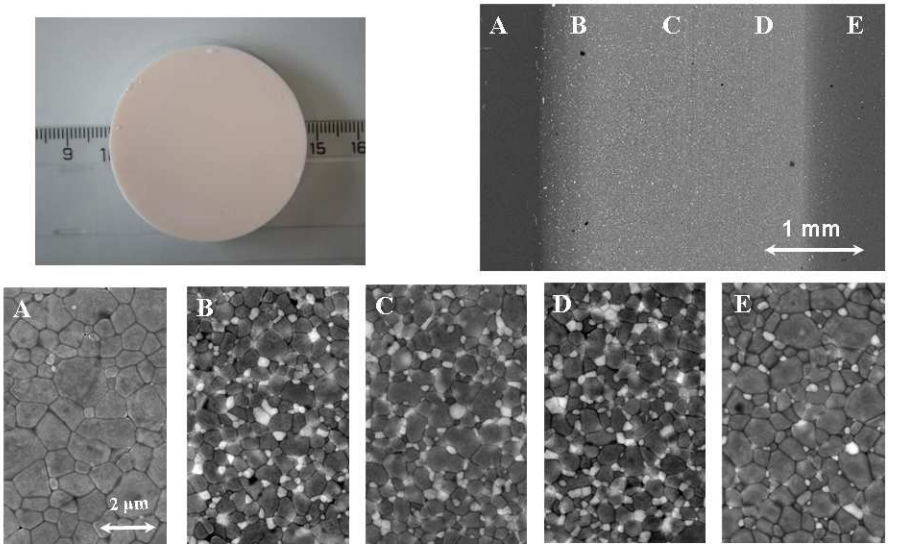

Figure 1. Graded microstructure of Al_2O_3/Y-ZrO_2 ceramics. (Courtesy of J. Vleugels, K.U. Leuven.)

efficient numerical schemes, such as specialized finite elements [Santare and Lambros 2000], boundary element techniques [Sutradhar and Paulino 2004], meshless methods [Ching and Chen 2007], and local integral equations [Sládek et al. 2005]. Thanks to their simplicity, these methods can be rather easily generalized to more complex issues such as coupled thermal-mechanical problems [Noda 1999] or crack propagation [Kandula et al. 2005]. Although this approach is very appealing from the computational point of view, its validity remains rather questionable as it contains no direct link to the underlying heterogeneous microstructure.

One possibility in establishing such a connection is to assert that the FGM locally behaves as a homogeneous composite characterized by a given volume fraction distribution and then use well established local effective media theories; see [Milton 2002; Böhm 2008] for more details. Local averaging techniques have attracted considerable attention due to their simplicity comparable to the previous class of models; see [Markworth et al. 1995; Cho and Ha 2001] for an overview and comparison of various local micromechanical models in the context of FGMs. An exemplary illustration of the capabilities of this modeling paradigm is the work [Goupee and Vel 2006] which provides an efficient algorithm for FGM composition optimization when taking into account coupled thermomechanical effects. Still, despite a substantial improvement in the physical relevance of the model, local averaging methods may lead to inaccurate results. This was demonstrated by systematic studies [Reiter et al. 1997; Reiter and Dvorak 1998], which clearly show that the local averaging technique needs to be adapted to the detailed character of the microstructure in a neighborhood of the point under consideration. When considering the local averaging techniques, however, such information is evidently not available as all the microstructural data was lumped into volume fractions only.

Another appealing approach to FGM modeling is an adaptive discrete modeling of the structure. In order to avoid the fully detailed problem, a simplified model based on, for example, local averaging

techniques is solved first. Then, in regions where the influence of the discreteness of the microstructure is most pronounced, the microstructure with all its details is recovered to obtain an accurate solution. Such a modeling strategy has been, for example, adopted in [Grujicic and Zhang 1998] when using the Voronoi cell finite element method, introduced by Ghosh et al. [1995] or more recently in [Vemaganti and Deshmukh 2006], in the framework of goal oriented modeling. Without a doubt, this approach yields the most accurate results for a given distribution of phases. However, its extension to include the inevitable randomness of the microstructure seems to be an open problem.

The systematic treatment of FGMs as random, statistically nonhomogeneous composites offers, on the other hand, a possibility to apply the machinery of statistical continuum mechanics [Beran 1968; Torquato 2001]. In this framework, overall response of the media is interpreted using the ensemble, rather then spatial, averages of the involved quantities. The first class of methods stems from the description of the material composition by a nonstationary random field. This approach was pioneered by Ferrante and Graham-Brady [2005] and further refined in [Rahman and Chakraborty 2007], where the random field description was applied to the volume fractions of the involved phases and the overall statistics were obtained using local averaging methods. Such a strategy, however, inevitably leads to the same difficulties as in the case of deterministic analysis with a given variation of volume fractions. Alternative methods exploit the tools of mechanics of heterogeneous media. This gives rise to a correct treatment of nonlocal effects when combined with appropriate techniques for estimating the statistics of local fields. Examples of FGM oriented studies include the work of Buryachenko and Rammerstorfer [2001] who employ the multiparticle effective field method or the study by Luciano and Willis [2004] based on the Hashin–Shtrikman energy principles; see also [Buryachenko 2007] for a comprehensive list of references in this field. Both works, however, being analytically based, concentrate on deriving explicit constitutive equations for FGMs and therefore work with infinite bodies neglecting the finite size of the microstructure.

The goal of this paper is to make the first step in formulating a numerical model which is free of the above discussed limitations. The microstructural description is systematically derived from a fully penetrable sphere model introduced by Quintanilla and Torquato [1997], which is briefly reviewed in Section 2. The statistics of local fields then follow from reformulation of the Hashin–Shtrikman (H–S) variational principles introduced, for example, in [Willis 1977; Willis 1981] and summarized in the current context in Section 3 together with the Galerkin scheme allowing us to treat general bodies proposed by Luciano and Willis [2005] or Procházka and Šejnoha [2003]. Section 4 covers the application of the finite element method (FEM) following [Luciano and Willis 2005; Luciano and Willis 2006] and the boundary element method (BEM) in the spirit of [Procházka and Šejnoha 2003]. Finally, based on results of a parametric study executed in Section 5, the comparison of both numerical schemes when applied to FGM modeling is performed in Section 6 together with a discussion of future improvements of the model. In order to make the presentation self-contained and to minimize technicalities, the attention is restricted to an one-dimensional elasticity problem (or, equivalently, to a simple laminate subject to body forces varying in one direction [Luciano and Willis 2001]).

In the following text, we adopt the matrix notation commonly used in the finite element literature. Hence, a, $\boldsymbol{a}$ and $\mathbf{A}$ denote a scalar quantity, a vector (column matrix), and a general matrix, respectively. Other symbols and abbreviations are introduced in the text as needed.

2. Microstructural model

As already indicated, the morphological description adopted in this work is the one-dimensional case of a microstructural model studied in [Quintanilla and Torquato 1997]. A particular realization can be depicted as a collection of N rods of length ℓ distributed within a structure of length L, see Figure 2. The position of the i-th rod is specified by the x coordinate of its *reference point* x_i, which in our case coincides with the midpoint of a rod.

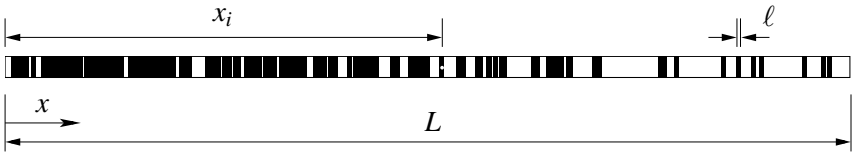

Figure 2. Example of microstructural model realization.

The microstructure gradation is prescribed by an *intensity function* $\rho(x)$, with the product $\rho(x)\,\mathrm{d}x$ giving the expected number of reference points in an infinitesimal neighborhood around x. Using the theory of general Poisson processes, the probability of finding exactly m points located in a finite-sized interval I is given by Quintanilla and Torquato [1997]

$$P_m(I) = \frac{\mu_\rho(I)^m}{m!}\exp\bigl(-\mu_\rho(I)\bigr), \quad \text{with} \quad \mu_\rho(I) = \int_I \rho(x)\,\mathrm{d}x. \tag{1}$$

Further, to provide a suitable framework for the description of the microstructure related to the model, we attach the symbol α to a particular microstructure realization (see Figure 2) from a sample space $\mathbb{S}$ endowed with a probability measure p. Then, the ensemble average of a random function $f(x,\alpha)$ is defined as[1]

$$\langle f\rangle(x) = \int_{\mathbb{S}} f(x,\alpha)\,p(\alpha)\,\mathrm{d}\alpha.$$

Now, interpret Figure 2 as a distribution of *white* and *black phases*. For a given configuration α, the distribution of a phase r is described by the characteristic function $\chi_r(x;\alpha)$ as

$$\chi_r(x;\alpha) = \begin{cases} 1 \text{ if } x \text{ is located in phase } r, \\ 0 \text{ otherwise,} \end{cases} \tag{2}$$

where $r = 1$ is reserved for the white phase (matrix) while $r = 2$ denotes the black phase (rod). The elementary statistical characterization of the model is provided by the *one-point probability function* S_r, defined as $S_r(x) = \langle\chi_r\rangle(x)$, giving the probability of finding a point x included in the phase r. Recognizing that the probability of locating x in the white phase coincides with the probability that the interval $I(x) = [x-\ell/2, x+\ell/2]$ will not be occupied by any reference point and using (1), we obtain

$$S_1(x) = P_0\bigl(I(x)\bigr) = \exp\biggl(-\int_{x-\ell/2}^{x+\ell/2}\rho(t)\,\mathrm{d}t\biggr).$$

[1]To simplify the exposition, we introduce the following notation: for a real-valued *random* function $f(x,\alpha):\mathbb{R}\times\mathbb{S}\to\mathbb{R}$, by writing $f(x;\alpha)$ we mean a *deterministic* function of $x\in\mathbb{R}$ related to a given *fixed* realization (that is, $f(x;\alpha):\mathbb{R}\to\mathbb{R}$). In other words, $f(x;\alpha) := f(x,\beta)|_{\beta=\alpha}$.

The one-point probability function $S_2(x)$ follows from the identity

$$S_1(x) + S_2(x) = 1, \tag{3}$$

which is a direct consequence of the adopted definition of the characteristic function; recall (2).

By analogy, we can introduce the *two-point* probability function S_{rs} as

$$S_{rs}(x, y) = \int_{\mathbb{S}} \chi_r(x, \alpha)\chi_s(y, \alpha)p(\alpha)\,\mathrm{d}\alpha,$$

quantifying the probability that a point x will be located in phase r while y stays in the phase s. For $r = s = 1$, the descriptor coincides with the probability that the union of intervals $I(x)$ and $I(y)$ will not be occupied by a reference point, yielding

$$S_{11}(x, y) = P_0\big(I(x) \cup I(y)\big). \tag{4}$$

The remaining functions S_{rs} can be directly expressed from S_{11} by exploiting identity (3). In particular:

$$\begin{aligned} S_{12}(x, y) &= S_1(x) - S_{11}(x, y), \\ S_{21}(x, y) &= S_1(y) - S_{11}(x, y), \\ S_{22}(x, y) &= 1 - S_1(x) - S_1(y) + S_{11}(x, y). \end{aligned}$$

Finally, to provide a concrete example, consider a piecewise linear intensity function

$$\rho(x) = \begin{cases} \rho_a, & 0 \le x \le a, \\ \rho_a + k_\rho(x - a), & a < x \le b, \\ \rho_b, & b < x \le L, \\ 0, & \text{otherwise}, \end{cases}$$

where $k_\rho = (\rho_b - \rho_a)/(b - a)$. The corresponding one- and two-point probability functions, evaluated using an adaptive Simpson quadrature [Gander and Gautschi 2000], are shown in Figure 3. Obviously,

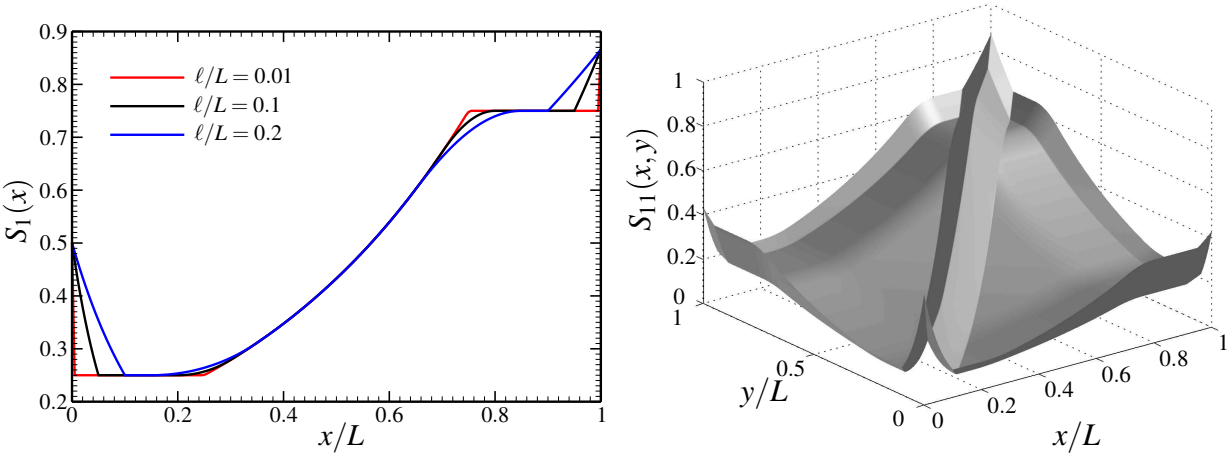

Figure 3. One-point (left) and two-point (right) probability functions for $a = 0.25L$, $b = 0.75L$, $L = 1$ m, $\rho_a = -\log(0.25/\ell)$ and $\rho_b = -\log(0.75/\ell)$. On the right, $\ell = 0.1$.

the shape of the one-point probability function directly follows from the intensity profile (up to some boundary effects due to the extension of ρ by zero outside of Ω and smoothing phenomena with the length scale ℓ demonstrating the "geometrical" size effect present in the model). The two-point probability function then contains further details of the distribution of individual constituents.

3. Hashin–Shtrikman variational principles

The geometrical description introduced provides a solid basis for the formulation of a stochastic model of one-dimensional binary functionally graded bodies. We will concentrate on the simplest case of linear elasticity with deterministic properties of single components.

3.1. ***Problem statement.*** Consider a bar of cross-sectional area 1 m^2, represented by the interval $\Omega = (0, L)$ with the boundaries $\partial\Omega = \{0, L\}$, fixed at $\partial\Omega^u$, subject to a body force $b(x)$ and tractions $\bar{t}$ at $\partial\Omega^t$ (see Figure 4). For a given realization α, the displacement field $u(x;\alpha)$ follows from the energy minimization problem $u(x;\alpha) = \arg\min_{v(x)\in\mathbb{V}} \Pi(v(x);\alpha)$, where $\arg\min_{x\in X} f(x)$ denotes the minimizer of f on X, $\mathbb{V}$ is the *realization-independent* set of kinematically admissible displacements, v is a test displacement field, and the energy functional Π is defined as

$$\Pi\big(v(x);\alpha\big) = \tfrac{1}{2}\int_\Omega \varepsilon\big(v(x)\big)E(x;\alpha)\varepsilon\big(v(x)\big)\,\mathrm{d}x - \int_\Omega v(x)b(x)\,\mathrm{d}x - \big(v(x)\bar{t}(x)\big)\Big|_{\partial\Omega^t},$$

with the strain field $\varepsilon(v(x)) = \dfrac{\mathrm{d}v}{\mathrm{d}x}(x)$ and the Young modulus E in the form

$$E(x;\alpha) = \chi_1(x;\alpha)E_1 + \chi_2(x;\alpha)E_2, \tag{5}$$

where E_i denotes the deterministic Young modulus of the i-th phase.

Now, given the probability distribution $p(\alpha)$, the ensemble average of displacement fields follows from the variational problem [Luciano and Willis 2005]:

$$\langle u\rangle(x) = \int_{\mathbb{S}} \Big(\arg\min_{v(x,\alpha)\in\mathbb{V}\times\mathbb{S}} \Pi\big(v(x),\alpha\big)\Big)\,p(\alpha)\,\mathrm{d}\alpha. \tag{6}$$

In theory, the previous relation fully specifies the distribution of displacement fields. The exact specification of the set $\mathbb{S}$ is, however, very complex and the probability distribution $p(\alpha)$ is generally not known. Therefore, the solution needs to be based on partial geometrical data such as the one- and two-point probability functions introduced in Section 2.

3.2. ***Hashin–Shtrikman decomposition.*** Following the seminal ideas of Hashin and Shtrikman [1962] and Willis [1977], the solution of the stochastic problem is sought as a superposition of two auxiliary problems, each characterized by constant material data E^0.

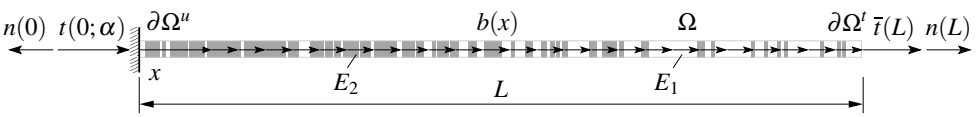

Figure 4. The one-dimensional elasticity problem associated with realization α.

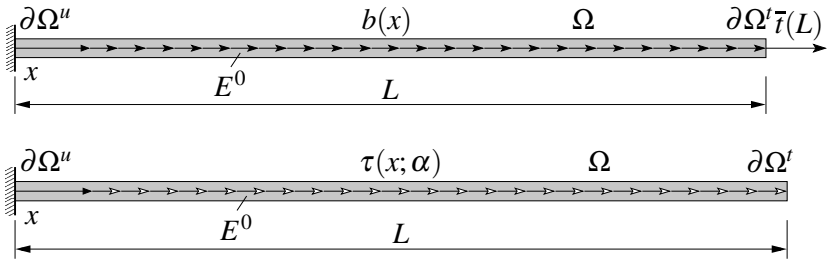

Figure 5. Problem decomposition: top, *deterministic* reference case; bottom, *stochastic* polarization problem.

In the first reference case (Figure 5, top), the homogeneous structure is subject to the body force b and the boundary tractions $\bar{t}$. The second, the polarization problem shown in Figure 5, bottom, corresponds to a homogeneous body loaded by polarization stress τ arising from the stress equivalence conditions $\sigma(x;\alpha) = E(x;\alpha)\varepsilon(x;\alpha) = E^0\varepsilon(x;\alpha) + \tau(x;\alpha)$. The unknown polarization stress now becomes a new variable to be determined as the stationary point of the two-field Hashin–Shtrikman–Willis functional (see [Willis 1977; Procházka and Šejnoha 2004] and [Bittnar and Šejnoha 1996, Chapter 1.8], for example)

$$\big(u(x;\alpha), \tau(x;\alpha)\big) = \arg \min_{v(x)\in\mathbb{V}} \operatorname*{stat}_{\theta(x;\alpha)\in\mathbb{T}(\alpha)} U\big(v(x), \theta(x;\alpha);\alpha\big), \tag{7}$$

where θ denotes an admissible polarization stress from the *realization-dependent* set $\mathbb{T}(\alpha)$, $\arg \operatorname*{stat}_{x\in X} f(x)$ stands for a stationary point of f on X, and a new energy functional U is defined as

$$U\big(v(x), \theta(x;\alpha);\alpha\big) = \frac{1}{2}\int_\Omega \varepsilon\big(v(x)\big) E^0 \varepsilon\big(v(x)\big)\,\mathrm{d}x - \int_\Omega v(x) b(x)\,\mathrm{d}x - \big(v(x)\bar{t}(x)\big)\Big|_{\partial\Omega^t} + \int_\Omega \theta(x;\alpha)\varepsilon\big(v(x)\big)\,\mathrm{d}x + \frac{1}{2}\int_\Omega \theta(x;\alpha)\big(E(x;\alpha) - E^0\big)^{-1}\theta(x;\alpha)\,\mathrm{d}x. \tag{8}$$

The minimization with respect to v in (7) can be efficiently performed using the Green's function technique. To that end, we introduce a decomposition of the displacement field

$$u(x;\alpha) = u^0(x) + u^1(x;\alpha), \tag{9}$$

where u^0 solves the reference problem, while u^1 denotes the displacement field due to a test stress polarization field θ. Note that the determination of u^0 is a standard task, which can be generally solved by a suitable numerical technique (see Sections 4.1 and 4.2). By introducing the Green's function of the reference problem satisfying

$$E^0 \frac{\partial^2 G^0}{\partial x^2}(x, y) + \delta(x - y) = 0,$$

with boundary conditions (n denotes the outer normal, recall Figure 4)

$$G^0(x, y) = 0 \text{ for } x \in \partial\Omega^u, \qquad T^0(x, y) = E^0 \frac{\partial G^0(x, y)}{\partial x} n(x) = 0 \text{ for } x \in \partial\Omega^t, \tag{10}$$

we relate the u^1 component and the associated strain field ε^1 to the polarization stresses θ via [Luciano and Willis 2005]

$$\begin{aligned} u^1(x;\alpha) &= -\int_\Omega \frac{\partial G^0(x,y)}{\partial y}\,\theta(y;\alpha)\,\mathrm{d}y = -\int_\Omega \Delta^0(x,y)\theta(y;\alpha)\,\mathrm{d}x, \\ \varepsilon\big(u^1(x;\alpha)\big) &= -\int_\Omega \frac{\partial^2 G^0(x,y)}{\partial x\partial y}\theta(y;\alpha)\,\mathrm{d}y = -\int_\Omega \Gamma^0(x,y)\theta(y;\alpha)\,\mathrm{d}x. \end{aligned} \tag{11}$$

By exploiting the optimality properties of the minimizing displacement $u(x;\alpha)$ and upon exchanging the order of optimization, Equation (8) can be, after some steps described in, for example, [Willis 1981; Luciano and Willis 2005], recast solely in terms of the polarizations

$$\tau(x;\alpha) = \arg \operatorname*{stat}_{\theta(x;\alpha)\in\mathbb{T}(\alpha)} H\big(\theta(x;\alpha);\alpha\big),$$

where the *condensed* energy functional is defined as

$$\begin{aligned} H\big(\theta(x;\alpha);\alpha\big) = \min_{v(x)\in\mathbb{V}} U\big(v(x),\theta(x;\alpha);\alpha\big) &= \Pi^0(u^0(x)) + \int_\Omega \theta(x;\alpha)\varepsilon\big(u^0(x)\big)\,\mathrm{d}x \\ &- \frac{1}{2}\int \theta(x;\alpha)\big(E(x;\alpha)-E^0\big)^{-1}\theta(x;\alpha)\,\mathrm{d}x - \frac{1}{2}\int_\Omega\int_\Omega \theta(x;\alpha)\Gamma^0(x,y)\theta(y;\alpha)\,\mathrm{d}x\,\mathrm{d}y, \end{aligned}$$

with Π^0 denoting the total energy of the reference structure.

With the Hashin–Shtrikman machinery at hand, the stochastic problem introduced by (6) can be solved by repeating the previous arguments in the probabilistic framework. In particular, taking the ensemble average of (9) and $(11)_1$ yields

$$\langle u\rangle(x) = u^0(x) - \int_\Omega \Delta^0(x,y)\langle\tau\rangle(y)\,\mathrm{d}y, \tag{12}$$

where the expectation $\langle\tau\rangle$ is a solution of the variational problem

$$\langle\tau\rangle(x) = \int_{\mathbb{S}} \big(\arg \operatorname*{stat}_{\theta(x,\alpha)\in\mathbb{T}(\alpha)\times\mathbb{S}} H(\theta(x,\alpha),\alpha)\big)\,p(\alpha)\,\mathrm{d}\alpha. \tag{13}$$

Again, due to limited knowledge of the detailed statistical characterization of the phase distribution, the previous variational problem can only be solved approximately. In particular, we postulate the following form of the polarization stresses:

$$\begin{aligned} \tau(x,\alpha) &\approx \chi_1(x,\alpha)\tau_1(x) + \chi_2(x,\alpha)\tau_2(x), \\ \theta(x,\alpha) &\approx \chi_1(x,\alpha)\theta_1(x) + \chi_2(x,\alpha)\theta_2(x), \end{aligned}$$

where τ_r and θ_r are now the realization-independent polarization stresses related to the r-th phase. Plugging the approximation into (13) leads, after some manipulations detailed in [Willis 1981; Šejnoha and

Zeman 2000], to the variational principle

$$\big(\tau_1(x),\,\tau_2(x)\big) = \arg \operatorname*{stat}_{(\theta_1(x),\theta_2(x))} \Pi^0\big(u^0(x)\big) + \sum_{r=1}^{2} \int_\Omega \theta_r(x) S_r(x) \varepsilon\big(u^0(x)\big)\,\mathrm{d}x$$
$$- \frac{1}{2}\sum_{r=1}^{2} \int_\Omega \theta_r(x) S_r(x)(E_r - E^0)^{-1}\theta_r(x)\,\mathrm{d}x - \frac{1}{2}\sum_{r=1}^{2}\sum_{s=1}^{2} \int_\Omega\int_\Omega \theta_r(x) S_{rs}(x,\,y)\Gamma^0(x,\,y)\theta_s(y)\,\mathrm{d}x\,\mathrm{d}y,$$

meaning that the *true* phase polarization stresses τ_r satisfy the optimality conditions ($r = 1, 2$)

$$\int_\Omega \theta_r(x) S_r(x)(E_r - E^0)^{-1}\tau_r(x)\,\mathrm{d}x$$
$$+ \sum_{s=1}^{2} \int_\Omega\int_\Omega \theta_r(x) S_{rs}(x,\,y)\Gamma^0(x,\,y)\tau_s(y)\,\mathrm{d}y\,\mathrm{d}x = \int_\Omega \theta_r(x) S_r(x)\varepsilon\big(u^0(x)\big)\,\mathrm{d}x, \quad (14)$$

for arbitrary θ_r.

3.3. ***Discretization.*** Two ingredients are generally needed to convert the conditions (14) to the finite-dimensional system: representation of the reference strain field and the Green's function-related quantities and discretization of the phase polarization stresses. The first step is dealt with in detail in Section 4; now it suffices to consider the approximations $\varepsilon^{0,h_0}(x)$, $\Delta^{0,h_0}(x)$ and $\Gamma^{0,h_0}(x,\,y)$, where h_0 denotes a parameter related to the discretization of the reference problem.[2]

Next, we reduce (14) to a finite-dimensional format using the standard Galerkin procedure. To that end, we introduce the discretization of the phase polarization stresses

$$\tau_r(x) \approx \mathbf{N}^{\tau h_1}(x)\boldsymbol{d}_r^{\tau h_0 h_1}, \qquad \theta_r(x) \approx \mathbf{N}^{\tau h_1}(x)\boldsymbol{d}_r^{\theta h_1}, \quad (15)$$

where $\mathbf{N}^{\tau h_1}$ is the matrix of (possibly discontinuous) shape functions controlled by the discretization parameter h_1; $\boldsymbol{d}_r^{\theta h_1}$ and $\boldsymbol{d}_r^{\tau h_0 h_1}$ denote the DOFs of trial and true polarization stresses, the latter related to the discrete Green's function. Introducing the approximations (15) in the variational statement (14) and using the arbitrariness of $\boldsymbol{d}_r^{\theta h_1}$ leads to a system of linear equations

$$\mathbf{K}_r^{\tau h_1}\boldsymbol{d}_r^{\tau h_0 h_1} + \sum_{s=1}^{2} \mathbf{K}_{rs}^{\tau h_0 h_1}\boldsymbol{d}_s^{\tau h_0 h_1} = \boldsymbol{R}_r^{\tau h_0 h_1}, \quad (16)$$

with the individual terms given by ($r, s = 1, 2$)

$$\mathbf{K}_r^{\tau h_1} = \int_\Omega \mathbf{N}^{\tau h_1}(x)^{\mathsf{T}} S_r(x)[E_r - E^0]^{-1}\mathbf{N}^{\tau h_1}(x)\,\mathrm{d}x, \quad (17)$$

$$\mathbf{K}_{rs}^{\tau h_0 h_1} = \int_\Omega\int_\Omega \mathbf{N}^{\tau h_1}(x)^{\mathsf{T}} S_{rs}(x,\,y)\Gamma^{0,h_0}(x,\,y)\mathbf{N}^{\tau h_1}(y)\,\mathrm{d}x\,\mathrm{d}y, \quad (18)$$

$$\boldsymbol{R}_r^{\tau h_0 h_1} = \int_\Omega \mathbf{N}^{\tau h_1}(x)^{\mathsf{T}} S_r(x)\varepsilon^{0,h_0}(x)\,\mathrm{d}x. \quad (19)$$

[2]To be more precise, the goal is not to obtain accurate estimates of the Green's function-related operators themselves, but rather to approximate the action of the operators; see Section 5.2 for further discussion.

Finally, once the approximate values of phase polarization stresses are available, the elementary statistics of the displacement field follow from the discretized form of (12):

$$\langle u\rangle(x) \approx \langle u\rangle^{h_0h_1}(x) = u^{0,h_0}(x) - \sum_{r=1}^{2}\left(\int_\Omega \Delta^{0,h_0}(x,y)S_r(y)\mathbf{N}^{\tau h_1}(y)\,\mathrm{d}y\right)\boldsymbol{d}_r^{\tau h_0 h_1}. \tag{20}$$

Note that additional information such as conditional statistics can be extracted from the polarization fields in postprocessing steps similar to (20); see [Luciano and Willis 2005; 2006] for more details.

4. Reference problem and Green's function-related quantities

4.1. ***Finite element method.*** The solution of the reference problem follows the standard finite element procedures, see for examples [Bittnar and Šejnoha 1996; Krysl 2006]. Nevertheless, we briefly repeat the basic steps of the method for the sake of clarity.[3] The reference displacement u^0 follows from the identity

$$\int_\Omega \varepsilon\big(v(x)\big)E^0\varepsilon\big(u^0(x)\big)\,\mathrm{d}x = \int_\Omega v(x)b(x)\,\mathrm{d}x + \big(v(x)\bar{t}(x)\big)\Big|_{\partial\Omega^t}, \tag{21}$$

which should hold for any test function $v \in \mathbb{V}$. Within the conforming finite element approach, the unknown displacement u^0 and the test function v together with the associated strain field are sought in a finite-dimensional subspace $\mathbb{V}^{h_0} \subset \mathbb{V}$

$$u^0(x) \approx u^{0,h_0}(x) = \mathbf{N}^{uh_0}(x)\boldsymbol{d}^{uh_0}, \qquad v(x) \approx v^{h_0}(x) = \mathbf{N}^{uh_0}(x)\boldsymbol{d}^{vh_0}, \tag{22}$$

$$\varepsilon\big(u^0(x)\big) \approx \varepsilon\big(u^{0,h_0}(x)\big) = \mathbf{B}^{uh_0}(x)\boldsymbol{d}^{uh_0}, \qquad \varepsilon\big(v(x)\big) \approx \varepsilon\big(v^{h_0}(x)\big) = \mathbf{B}^{uh_0}(x)\boldsymbol{d}^{vh_0}, \tag{23}$$

where $\mathbf{N}^{uh_0}$ is the displacement interpolation matrix and $\mathbf{B}^{uh_0}$ denotes the displacement-to-strain matrix. Using the discretized fields, (21) reduces to the system

$$\mathbf{K}^{uh_0}\boldsymbol{d}^{uh_0} = \boldsymbol{R}^{uh_0}, \tag{24}$$

where

$$\mathbf{K}^{uh_0} = \int_\Omega \mathbf{B}^{uh_0}(x)^{\mathsf{T}}E^0\mathbf{B}^{uh_0}(x)\,\mathrm{d}x, \qquad \boldsymbol{R}^{uh_0} = \int_\Omega \mathbf{N}^{uh_0}(x)^{\mathsf{T}}b(x)\,\mathrm{d}x + \big(\mathbf{N}^{uh_0}(x)\bar{t}(x)\big)\Big|_{\partial\Omega^t}. \tag{25}$$

Solving the system for $\boldsymbol{d}^{uh_0}$ enables us to obtain the ε^{0,h_0} approximation using $(23)_1$.

The discretized version of the Green's function follows from (21) with $\bar{t} = 0$ and $b = \delta(y - x)$ (see (24) and $(25)_2$),

$$G^0(x,y) \approx G^{0,h_0}(x,y) = \mathbf{N}^{uh_0}(x)(\mathbf{K}^{uh_0})^{-1}\mathbf{N}^{uh_0}(y)^{\mathsf{T}}.$$

The remaining Green's function-related quantities can now be expressed directly from (11) and $(11)_2$, leading to

$$\Delta^0(x,y) \approx \Delta^{0,h_0}(x,y) = \mathbf{N}^{uh_0}(x)(\mathbf{K}^{uh_0})^{-1}\mathbf{B}^{uh_0}(y)^{\mathsf{T}}, \tag{26}$$

$$\Gamma^0(x,y) \approx \Gamma^{0,h_0}(x,y) = \mathbf{B}^{uh_0}(x)(\mathbf{K}^{uh_0})^{-1}\mathbf{B}^{uh_0}(y)^{\mathsf{T}}. \tag{27}$$

[3]Recall that for simplicity, we assume homogeneous Dirichlet boundary conditions only. The treatment of the nonhomogeneous data can be found in [Luciano and Willis 2005, Appendix A].

4.2. ***Boundary element discretization.*** Following the standard BEM procedures (see for examples [Bittnar and Šejnoha 1996; Duddeck 2002]), we start from the Betti identity written for the reference problem

$$\int_\Omega \frac{\mathrm{d}^2 v}{\mathrm{d}\xi^2}(\xi) E^0 u^0(\xi)\,\mathrm{d}\xi = \big(n(\xi)\varepsilon(v(\xi))E^0 u^0(\xi) - v(\xi)t^0(\xi)\big)\Big|_{\partial\Omega(\xi)} - \int_\Omega v(\xi)b(\xi)\,\mathrm{d}\xi, \tag{28}$$

and apply the test displacement in the form $v(\xi) = G^{0,\infty}(\xi, x)$, where $G^{0,\infty}$ is the infinite body Green's function defined as the solution of

$$E^0 \frac{\partial^2 G^{0,\infty}(\xi, x)}{\partial \xi^2} + \delta(x-\xi) = 0, G^{0,\infty}(\xi, x) = G^{0,\infty}(x, \xi). \tag{29}$$

In the one-dimensional setting, this quantity is provided by [Luciano and Willis 2001, Equation (13)]

$$G^{0,\infty}(x,\xi) = -\frac{1}{2E^0}|x-\xi|,$$

and the integral identity (28), written for any $x \in \Omega$, receives the form

$$u^{0,h_0}(x) = \big(G^{0,\infty}(x,\xi)t^{0,h_0}(\xi) - T^{0,\infty}(x,\xi)u^{0,h_0}(\xi)\big)\Big|_{\partial\Omega(\xi)} + \int_\Omega G^{0,\infty}(x,\xi)b(\xi)\,\mathrm{d}\xi, \tag{30}$$

where the tractions $T^{0,\infty}(x,\xi)$ are defined analogously to $(10)_2$ as

$$T^{0,\infty}(x,\xi) = E^0 \frac{\partial G^{0,\infty}(x,\xi)}{\partial \xi} n(\xi) = \big(H(x-\xi) - \tfrac{1}{2}\big)n(\xi), \quad \text{for} \quad \xi \in \partial\Omega, \tag{31}$$

and H denotes the Heaviside function. Imposing the consistency with boundary data for $x \to 0_+$ and $x \to L_-$ yields the system of two linear equations

$$E^0 u^{0,h_0}(L) - E^0 u^{0,h_0}(0) - L t^{0,h_0}(L) = \int_\Omega \xi b(\xi)\,\mathrm{d}\xi, \tag{32}$$

$$E^0 u^{0,h_0}(L) - E^0 u^{0,h_0}(0) - L t^{0,h_0}(0) = \int_\Omega (L-\xi) b(\xi)\,\mathrm{d}\xi. \tag{33}$$

Since one component of the pair (u^{0,h_0}, t^{0,h_0}) is always specified on $\partial\Omega$ and $\partial\Omega^u \neq \varnothing$, the previous system uniquely determines the unknown boundary data (that is, u^{0,h_0} on $\partial\Omega^t$ and t^{0,h_0} on $\partial\Omega^u$), needed to evaluate (30).[4]

Making use of the identity $2E^0\partial_x G^{0,\infty}(x,\xi) = 1 - 2H(x-\xi)$, the associated strain field can be expressed as

$$\begin{aligned}\varepsilon^{0,h_0}(x) &= \left(\frac{\partial G^{0,\infty}(x,\xi)}{\partial x} t^{0,h_0}(\xi)\right)\Big|_{\partial\Omega(\xi)} + \int_\Omega \frac{\partial G^{0,\infty}(x,\xi)}{\partial x} b(\xi)\,\mathrm{d}\xi \\ &= \frac{1}{2E^0}\left(t^{0,h_0}(L) - t^{0,h_0}(0) - \int_0^x b(\xi)\,\mathrm{d}\xi + \int_x^L b(\xi)\,\mathrm{d}\xi\right).\end{aligned} \tag{34}$$

[4]It can be verified that (30) now provides the exact *one-dimensional* displacement field rather than an approximate one. Nevertheless, to keep the following discussion valid in the multidimensional setting and consistent with Section 4.1, we keep the index "h_0" in the sequel.

Analogously to the finite element treatment, the expression for the finite-body Green's function starts from (28) with $b = \delta(y - \xi)$ and boundary data (10). Following the specific form of (30) (and allowing for a slight inconsistency in notation), we introduce a decomposition of the Green's function into the discretization-independent infinite-body part and the discretization-dependent boundary contribution $G^0(x, y) \approx G^{0,\infty}(x, y) + G^{0,h_0}(x, y)$, where the boundary part, written for $x \in \Omega$ and $y \in \Omega$, assumes the form

$$G^{0,h_0}(x, y) = \big(G^{0,\infty}(x, \xi)T^{0,h_0}(\xi, y) - T^{0,\infty}(x, \xi)G^{0,h_0}(\xi, y)\big)\Big|_{\partial\Omega(\xi)},$$

with the boundary displacements G^{0,h_0} and tractions T^{0,h_0} at $\xi \in \partial\Omega$ due to a unit impulse at y determined from a linear system (compare with (32) and (33))

$$E^0 G^{0,h_0}(L, y) - E^0 G^{0,h_0}(0, y) - L T^{0,h_0}(L, y) = y, \tag{35}$$

$$E^0 G^{0,h_0}(L, y) - E^0 G^{0,h_0}(0, y) - L T^{0,h_0}(0, y) = L - y. \tag{36}$$

The expression for Δ^0 is derived following an analogous procedure. We exploit the infinite-body–boundary split $\Delta^0(x, y) \approx \Delta^{0,\infty}(x, y) + \Delta^{0,h_0}(x, y)$, and obtain the first part directly from the definition (11)

$$\Delta^{0,\infty}(x, y) = \frac{\partial G^{0,\infty}(x, y)}{\partial y} = \frac{1}{2E^0}\big(2H(x - y) - 1\big).$$

The boundary-dependent part now follows from

$$\Delta^{0,h_0}(x, y) = \left(G^{0,\infty}(x, \xi)\frac{\partial T^{0,h_0}(\xi, y)}{\partial y} - T^{0,\infty}(x, \xi)\frac{\partial G^{0,h_0}(\xi, y)}{\partial y}\right)\Big|_{\partial\Omega(\xi)},$$

with the y-sensitivities of the boundary data evaluated from (35)–(36) as

$$E^0\frac{\partial G^{0,h_0}(L, y)}{\partial y} - E^0\frac{\partial G^{0,h_0}(0, y)}{\partial y} - L\frac{\partial T^{0,h_0}(L, y)}{\partial y} = 1, \tag{37}$$

$$E^0\frac{\partial G^{0,h_0}(L, y)}{\partial y} - E^0\frac{\partial G^{0,h_0}(0, y)}{\partial y} - L\frac{\partial T^{0,h_0}(0, y)}{\partial y} = -1. \tag{38}$$

The BEM-based approach is completed by approximating the Γ^0 function. In particular, we get

$$\Gamma^0(x, y) \approx \Gamma^{0,\infty}(x, y) + \Gamma^{0,h_0}(x, y), \tag{39}$$

$$\Gamma^{0,\infty}(x, y) = \frac{\partial \Delta^{0,\infty}(x, y)}{\partial x} = \frac{1}{E^0}\delta(x - y), \tag{40}$$

$$\begin{aligned}\Gamma^{0,h_0}(x, y) &= \frac{\partial \Delta^{0,h_0}(x, y)}{\partial x} = \left(\frac{G^{0,\infty}(x, \xi)}{\partial x}\frac{\partial T^{0,h_0}(\xi, y)}{\partial y}\right)\Big|_{\partial\Omega(\xi)} \\ &= \frac{1}{2E^0}\left(\frac{\partial T^{0,h_0}(L, y)}{\partial y} - \frac{\partial T^{0,h_0}(0, y)}{\partial y}\right).\end{aligned} \tag{41}$$

Finally note that the previous procedure can be directly translated to multidimensional and/or vectorial cases; see [Procházka and Šejnoha 2003, Section 3] for more details.

5. Numerical examples

Before getting to the heart of the matter, we start by converting the relations (16)–(20) to the fully discrete format by replacing the integrals by a numerical quadrature and selecting a specific form of shape functions $\mathbf{N}^{\tau h_1}$. To that end, we introduce a set of integration points $\{\zeta_1, \zeta_2, \ldots, \zeta_{N_\zeta}\}$ as well as associated integration weights $\{w_1, w_2, \ldots, w_{N_\zeta}\}$ and evaluate the components of the system matrix and right-hand side vector as

$$\mathbf{K}_r^{\tau h_1} \approx \sum_{i=1}^{N_\zeta} w_i \mathbf{N}^{\tau h_1}(\zeta_i)^{\mathsf{T}} S_r(\zeta_i)[E_r - E^0]^{-1} \mathbf{N}^{\tau h_1}(\zeta_i), \tag{42}$$

$$\mathbf{K}_{rs}^{\tau h_0 h_1} \approx \sum_{i=1}^{N_\zeta} \sum_{j=1}^{N_\zeta} w_i w_j \mathbf{N}^{\tau h_1}(\zeta_i)^{\mathsf{T}} S_{rs}(\zeta_i, \zeta_j) \Gamma^{0,h_0}(\zeta_i, \zeta_j) \mathbf{N}^{\tau h_1}(\zeta_j) + \int_\Omega \int_\Omega \mathbf{N}^{\tau h_1}(x)^{\mathsf{T}} S_{rs}(x, y) \Gamma^{0,\infty}(x, y) \mathbf{N}^{\tau h_1}(y)\, \mathrm{d}x\, \mathrm{d}y, \tag{43}$$

$$\boldsymbol{R}_r^{\tau h_0 h_1} \approx \sum_{i=1}^{N_\zeta} \mathbf{N}^{\tau h_1}(\zeta_i)^{\mathsf{T}} S_r(\zeta_i) \varepsilon^{0,h_0}(\zeta_i), \tag{44}$$

$$\langle u \rangle^{h_0 h_1}(x) \approx u^{0,h_0}(x) - \sum_{r=1}^{2} \sum_{i=1}^{N_\zeta} w_i \Delta^{0,h_0}(x, \zeta_i) S_r(\zeta_i) \mathbf{N}^{\tau h_1}(\zeta_i) \boldsymbol{d}_r^{\tau h_0 h_1} - \sum_{r=1}^{2} \left(\int_\Omega \Delta^{0,\infty}(x, y) S_r(y) \mathbf{N}^{\tau h_1}(y)\, \mathrm{d}y \right) \boldsymbol{d}_r^{\tau h_0 h_1}, \tag{45}$$

with the convention $\Gamma^{0,\infty} = \Delta^{0,\infty} \equiv 0$ for the FEM-based approximation of the polarization problem. The basis functions and integration schemes employed below, based on a uniform partitioning of Ω into N_e cells Ω_e of length $h_1 = L/N_e$, are defined by Figure 6. In particular, the specification of the polarization stress in terms of $\mathbb{P}_0$ shape functions requires $2N_e$ DOFs (meaning one DOF per cell and phase), while the $\mathbb{P}_1$ and $\mathbb{P}_{-1}$ discretizations are parametrized using $2(N_e + 1)$ or $4N_e$ values, respectively.

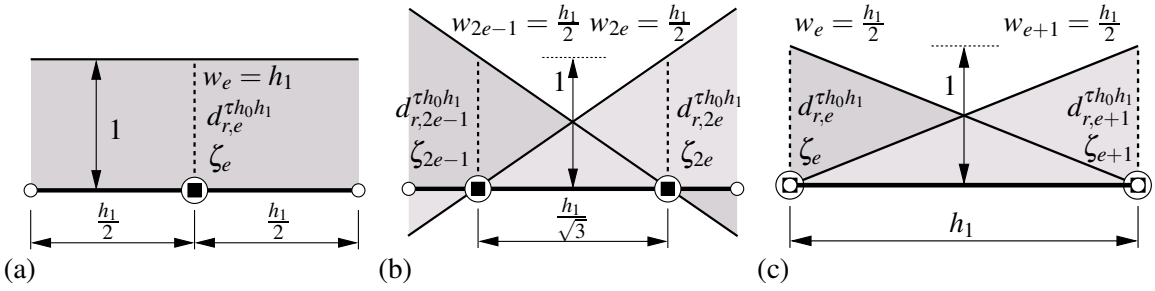

Figure 6. Choice of shape functions and integration points related to the e-th cell: (a) piecewise-constant basis functions ($\mathbb{P}_0$) and the Gauss–Legendre quadrature of order 1 (GL_1), (b) piecewise-linear discontinuous basis functions ($\mathbb{P}_{-1}$) and the Gauss–Legendre quadrature of order 2 (GL_2), and (c) piecewise linear continuous basis functions ($\mathbb{P}_1$) and Newton–Cotes quadrature of order 1 (NC_1). ∘ represent cell nodes, ◯ degrees of freedom, and ■ integration points.

Note that the BEM-related infinite-body contributions appearing in (43) and (45) are still kept explicit, as they are available in the closed form and can be treated separately. In the present case, action of the $\Gamma^{0,\infty}$ operator is local — recall (41) — while the quantities related to $\Delta^{0,\infty}$ are evaluated at cell nodal points and linearly interpolated to the interior of a cell to account for the discontinuity of the integrand.

To summarize, the following factors significantly influence the accuracy of the discrete Hashin–Shtrikman scheme:

- approximation of the Green's function of the comparison body,
- the basis functions and numerical quadrature used to discretize the polarization problem,
- the Young's modulus of the reference body E^0,
- contrast of the Young moduli of individual phases (E_2/E_1),
- the characteristic size of the microstructure with respect to the analyzed domain (ℓ/L).

All these aspects are studied in detail in the rest of this section. Two representative examples of structures subject to a uniform body force b and homogeneous mixed and Dirichlet boundary data are considered, see Figure 7,

$$\text{statically determinate structure:} \quad u(0,\alpha)=0, \quad t(L,\alpha)=0, \tag{46}$$

$$\text{statically indeterminate structure:} \quad u(0,\alpha)=0, \quad u(L,\alpha)=0. \tag{47}$$

In both cases, the heterogeneity distribution is quantified according to the model introduced in Section 2 with the one- and two-point probability functions plotted in Figure 3. Moreover, taking advantage of the one-dimensional setting, we systematically compare the obtained numerical results against reliable reference values determined by extensive Monte Carlo (MC) simulations, introduced next.

5.1. ***Direct simulation results.*** For the purpose of the following discussion, the reference values of the average displacement fields $\langle u\rangle_{\mathrm{MC}}(x)$ together with the 99.9% interval estimates $[\langle u_-\rangle_{\mathrm{MC}}(x), \langle u_+\rangle_{\mathrm{MC}}(x)]$ are understood as the piecewise linear interpolants of discrete data sampled by the MC procedure described in detail in the Appendix. In addition, the homogenized displacement field $u_{\mathrm{H}}(x)$, corresponding to a deterministic structure with the position-dependent elastic modulus

$$\frac{1}{E_{\mathrm{H}}(x)} = \frac{S_1(x)}{E_1} + \frac{S_2(x)}{E_2}, \tag{48}$$

is introduced to assess the performance of the local averaging approach. Figure 7 stores several representative results plotted using dimensionless quantities.

As apparent from Figure 7, the obtained statistics of overall response exhibit rather narrow confidence intervals, implying the reliability and accuracy of the MC estimates. For the statically determinate structure, the locally homogenized solution coincides with the ensemble average of the displacement fields, as demonstrated by the overlap of the simulation results with the homogenized data. The converse is true (with the 99.9% confidence) for the statically indeterminate case, where these two results can be visually distinguished from each other. The mismatch (which increases with increasing E_2/E_1 or ℓ/L) clearly demonstrates that even in the one-dimensional setting local averaging may lead to incorrect values when treating nonhomogeneous random media. These results are consistent with the fact that

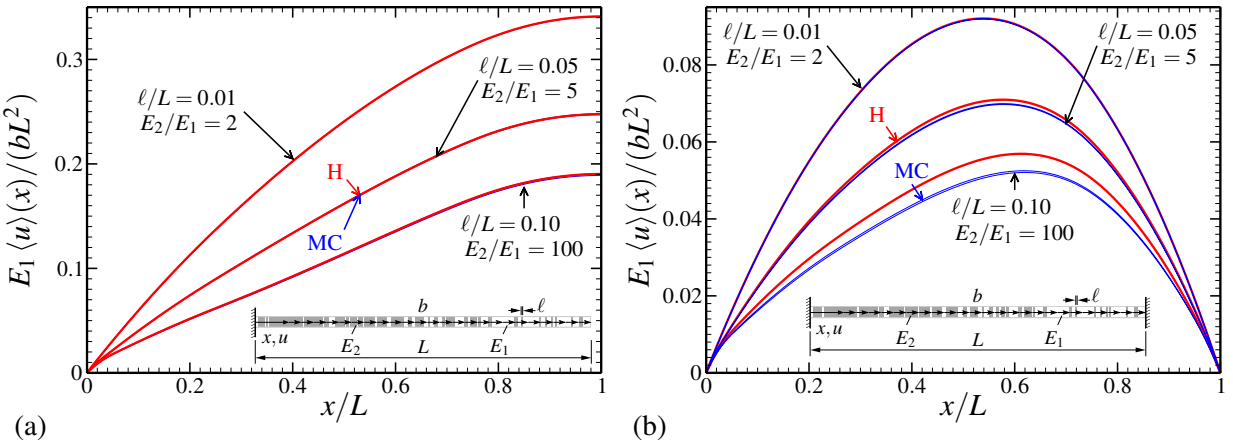

Figure 7. Reference MC solution; (a) statically determinate and (b) indeterminate problems; MC results correspond to 99.9% confidence interval estimates, H refers to homogenized solution.

in the statically determinate case, the stress field $\sigma(x,\alpha)$ is independent of α as follows from the one-dimensional equilibrium equations $\partial_x\sigma(x,\alpha)+b(x)=0$ and the deterministic value of the traction at $x=L$ due to the boundary condition provided by $(46)_2$. In the latter case, however, the traction value as well as the stress field become configuration-dependent. Such an effect does not appear in the classical homogenization setting, where for $\ell/L\to 0$ the harmonic average is known to represent the homogenized solution exactly [Murat and Tartar 1997]. This result naturally justifies the application of approaches based on higher-order statistics to FGMs, with the H–S method being the most prominent example.

5.2. ***Effect of the Green's function approximation.*** In order to illustrate the effect of the approximate Green's function, we restrict our attention to the statistically determinate structure and employ the standard piecewise linear basis functions $\mathbf{N}^{uh_0}$ to evaluate the Γ^{0,h_0} function in the FEM setting using (27). Figure 8 allows us to perform the qualitative assessment of the results for different choices of basis functions, integration schemes, and discretization parameters h_0.

Evidently, a suitable choice of discretization parameter h_0 is far from straightforward. From all the possibilities presented in Figure 8a, only the combinations $h_1=h_0$ with the $\mathbb{P}_0/\mathrm{GL}_1$ discretization of the polarization problem and $h_1=2h_0$ with the $\mathbb{P}_{-1}/\mathrm{GL}_2$ scheme are capable of reproducing the homogenized solution, while all the remaining possibilities lead to inaccurate results often accompanied by an oscillatory response. On the other hand, the h_0-independent BEM-based solutions show correct response for all discretizations of the polarization problem (and are virtually independent of the scheme used due to the sufficiently low value of the h_1 parameter, see Section 5.5).

To shed a light on such phenomena, consider the FEM approximation of the Γ^{0,h_0} function plotted in Figure 9a. The piecewise linear basis functions used to express the reference displacements imply the piecewise constant values of $\Gamma^{0,h_0}(x,y)$ approximating the exact expression $\frac{1}{E^0}\delta(x-y)$, see (39). As pointed out by Luciano and Willis [2006], however, the accuracy of the HS scheme is governed by the correct reproduction of the *action* of the $\Gamma^0(x,y)$ operator rather than the local values. In the present

context, it follows from (44) that such a requirement is equivalent to the accurate representation of the $\Gamma^0(x, y)$ operator action for x coinciding with the integration points related to the selected numerical quadrature. It can be verified that this condition is satisfied only for the two aforementioned discretizations of the reference problem. In particular, for the $\mathbb{P}_0/\mathrm{GL}_1$ combination we obtain (see Figures 9a and 10a)

$$\int_{\Omega_e} \Gamma^0(\zeta_e, \xi)\tau_r(\xi)\,\mathrm{d}\xi \approx w_e \Gamma^{0,h_0}(\zeta_e, \zeta_e) d_{e,r}^{\tau h_0 h_1} = h_1 \frac{1}{E^0 h_0} d_{e,r}^{\tau h_0 h_1} = \frac{d_{e,r}^{\tau h_0 h_1}}{E^0},$$

meaning that the numerical scheme reproduces the action of Γ^0 exactly.

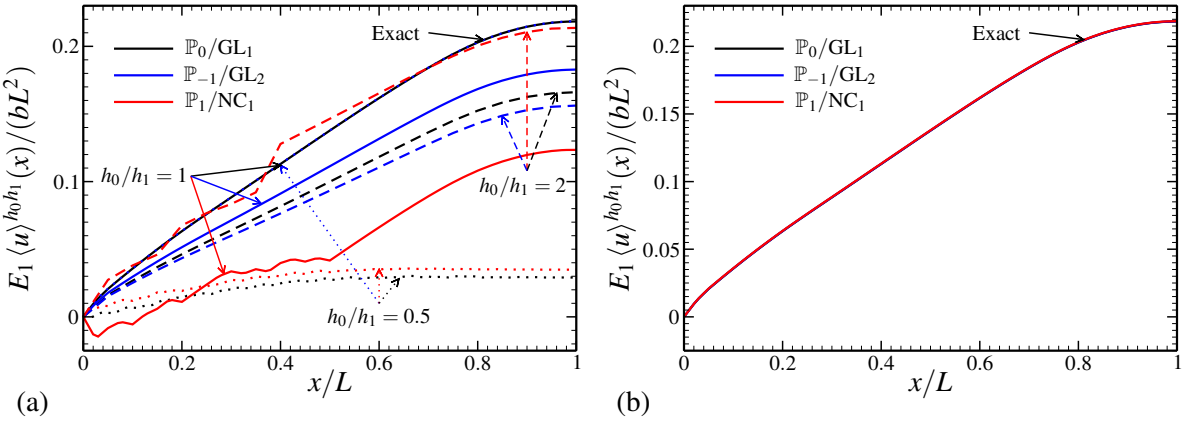

Figure 8. Influence of the approximate Green's function for the statically determinate problem: (a) FEM-based solution, and (b) BEM-based solution. $E_2/E_1 = 10$, $E^0/E_1 = 5$, $\ell/L = 0.1$, and $h_1/\ell = 0.25$.

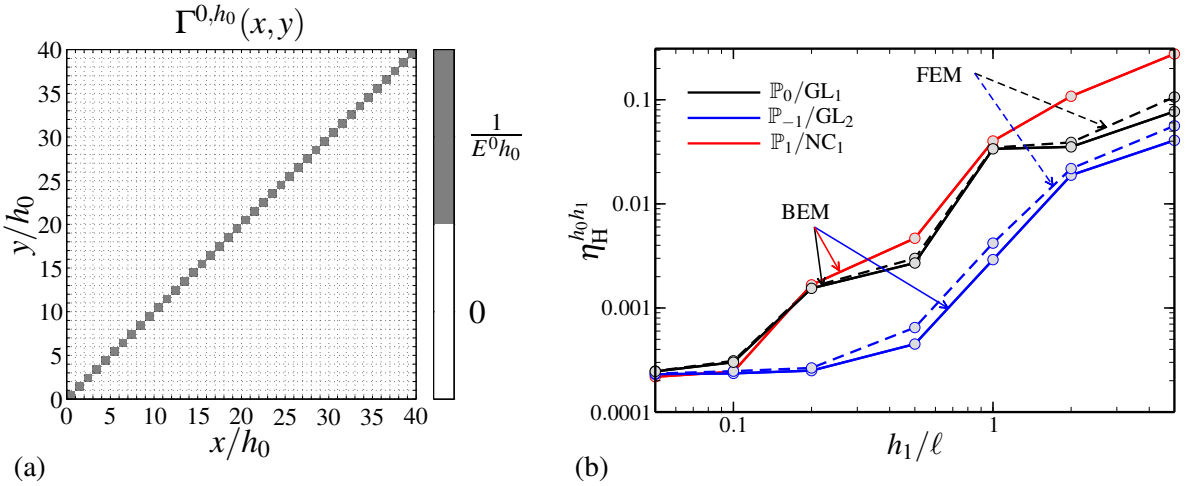

Figure 9. (a) Finite element approximation of the Green's function and (b) convergence rates of FEM vs. BEM; $E_2/E_1 = 10$, $E^0/E_1 = 5$, and $\ell/L = 0.1$.

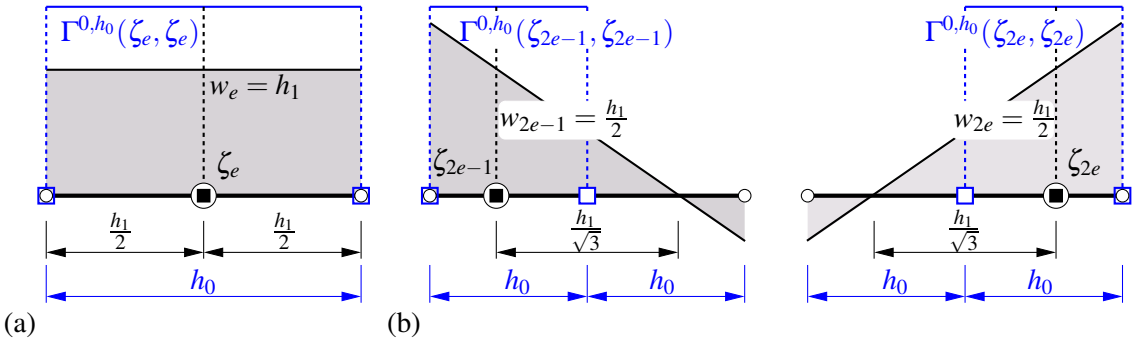

Figure 10. Valid combinations of the discretized Green's function and the polarization stresses: (a) $\mathbb{P}_0/\mathrm{GL}_1$ and (b) $\mathbb{P}_{-1}/\mathrm{GL}_2$; □ are finite element nodes.

Using Figures 9a and 10b, we find the analysis of the $\mathbb{P}_{-1}/\mathrm{GL}_2$ discretization completely analogous:

$$\int_{\Omega_e} \Gamma^0(\zeta_{2e-1},\xi)\tau_r(\xi)\,\mathrm{d}\xi \approx w_{2e-1}\Gamma^{0,h_0}(\zeta_{2e-1},\zeta_{2e-1})d^{\tau h_0 h_1}_{2e-1,r} = \frac{h_1}{2}\frac{1}{E^0 h_0}d^{\tau h_0 h_1}_{2e-1,r} = \frac{d^{\tau h_0 h_1}_{2e-1,r}}{E^0},$$

$$\int_{\Omega_e} \Gamma^0(\zeta_{2e},\xi)\tau_r(\xi)\,\mathrm{d}\xi \approx w_{2e}\Gamma^{0,h_0}(\zeta_{2e},\zeta_{2e})d^{\tau h_0 h_1}_{2e,r} = \frac{d^{\tau h_0 h_1}_{2e,r}}{E^0},$$

which explains the good performance of the particular discretization scheme.

To allow for the quantitative comparison, we exploit the fact that the exact solution is available for the statically determinate case and introduce a relative L_2 error measure

$$\eta_{\mathrm{H}}^{h_0 h_1} = \frac{\big\|\langle u\rangle^{h_0 h_1}(x) - u_{\mathrm{H}}(x)\big\|_{L_2(\Omega)}}{\big\|u_{\mathrm{H}}(x)\big\|_{L_2(\Omega)}}. \tag{49}$$

The resulting convergence rates of the FEM- and BEM-based approaches are shown in Figure 10b with the integrals in (49) evaluated using an adaptive Simpson quadrature [Gander and Gautschi 2000] with a relative accuracy of 10^{-6}. Clearly, the performance of the BEM-based scheme is slightly superior to the (properly tuned) FEM approach. By a sufficient resolution of the reference problem, however, both approaches become comparable. Moreover, the results confirm the good performance of the $\mathbb{P}_0$ and $\mathbb{P}_1$ schemes when compared to the $\mathbb{P}_{-1}$ discretization, which requires about twice the number of DOFs of the former schemes for the same cell dimensions h_1 (recall Figure 6). Similar conclusions can also be drawn for the statically indeterminate case. Therefore, in view of the above comments, we concentrate on the BEM approach in the sequel and limit the choice of basis functions to $\mathbb{P}_0$ and $\mathbb{P}_1$ only.

5.3. ***Influence of the integration scheme and basis functions.*** Thus far, we have investigated the combination of the *polarization* numerical quadratures and shape functions, for which the location of integration points coincides with the position of DOFs. Figure 11 shows the convergence plots for the relevant basis function/integration scheme pairs. To address also the statically determinate case, the relative error is

now related to the MC data, leading to the definition

$$\eta_{\mathrm{MC}}^{h_0 h_1} = \frac{\left\| \langle u \rangle^{h_0 h_1}(x) - \langle u \rangle_{\mathrm{MC}}(x) \right\|_{L_2(\Omega)}}{\left\| \langle u \rangle_{\mathrm{MC}}(x) \right\|_{L_2(\Omega)}}. \tag{50}$$

In addition, two comparative values are introduced: the relative error of the homogenized solution H (determined by (50) with $\langle u \rangle^{h_0 h_1}$ replaced by u_{H}) and the relative error associated with the $\langle u_- \rangle_{\mathrm{MC}}$ or $\langle u_+ \rangle_{\mathrm{MC}}$ function, appearing as the interval estimate (IE) line.

For the statistically determinate structure, the observed behavior is rather similar to the one reported in Section 5.2. In particular, Figure 11a confirms that the H–S solution quickly reaches an accuracy comparable with the confidence intervals (indicated by the grey area) and eventually converges to the homogenized solution, with the exception of the $\mathbb{P}_1/\mathrm{GL}_1$ combination resulting in a singular system matrix (16). Moreover, the superiority of the GL_2 quadrature over the lower-order scheme is evident; the proper representation of spatial statistics seems to be more important than smoothness of the polarization shape functions.

Figure 11b shows the results for the statically indeterminate case. With 99.9% confidence, the results *quantitatively* demonstrate that the homogenized solution differs from the MC data. The H–S solution gives an error of about 50% of the value of the homogenized solution, but ceases to attain the accuracy set by the confidence interval. It should be kept in mind that the H–S result actually delivers an estimate pertinent to the fixed value of parameter E^0 and *all* random one-dimensional media characterized by the two-point statistics (4).

5.4. ***Influence of the reference media and phase contrast.*** Having identified the intrinsic limitation of the H–S approach, we proceed with the last free parameter of the method: the choice of the reference medium. To that end, we introduce the parameterization of the Young modulus

$$E^0 = (1-\omega)E_1 + \omega E_2.$$

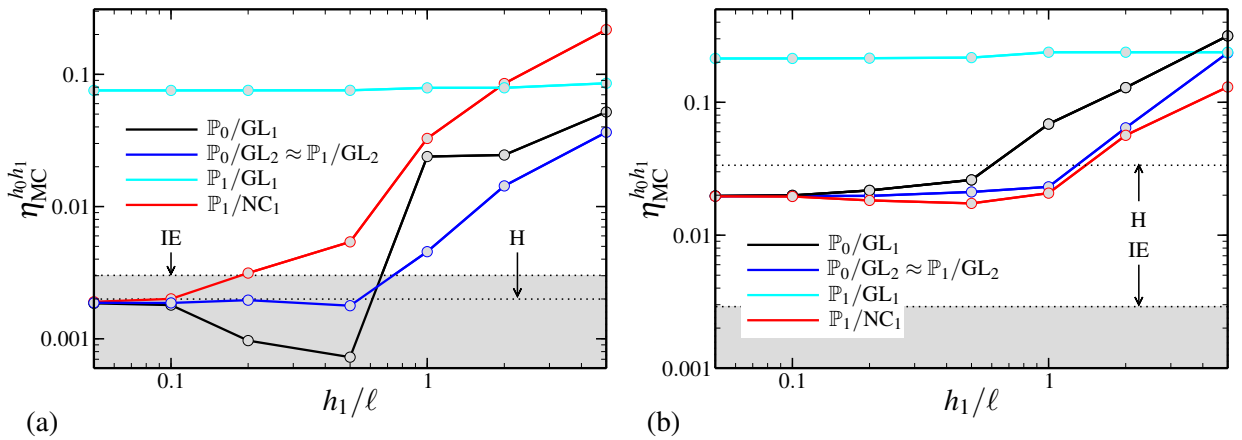

Figure 11. Influence of the choice of numerical discretization: (a) statically determinate and (b) indeterminate structures; $E_2/E_1 = 5$, $\ell/L = 0.1$, $E^0/E_1 = 3$, and IE denotes the error associated with the 99.9% confidence interval estimate.

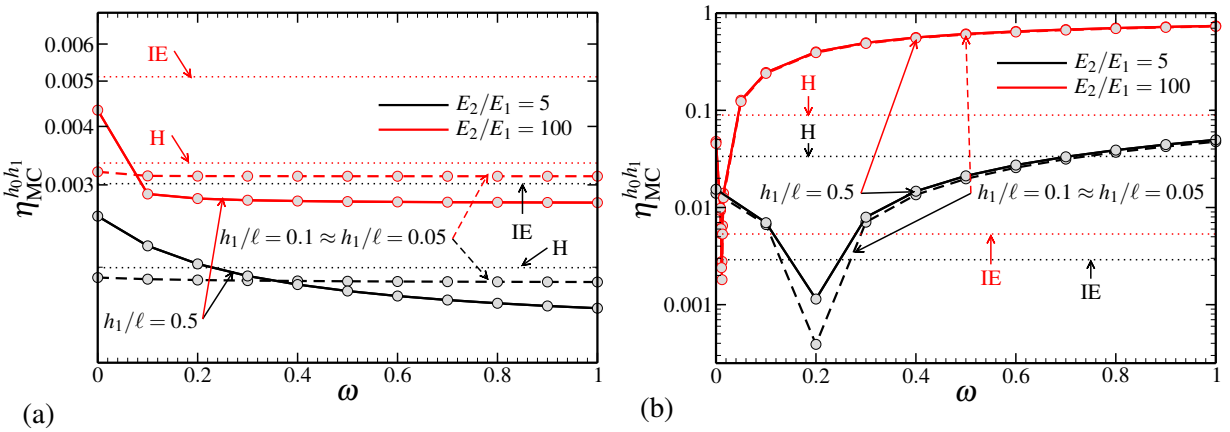

Figure 12. Influence of the choice of the reference media: (a) statically determinate and (b) indeterminate structures; $\ell/L = 0.1$, and $\mathbb{P}_0/\mathrm{GL}_2$ discretization.

Note that for the phases indexed such that $E_1 < E_2$, $\omega = 0$ and $\omega = 1$ correspond to the rigorous lower and upper bounds on the ensemble average of the energy stored in the structure and, consequently, to the positive- or negative-definite system matrix [Procházka and Šejnoha 2004; Luciano and Willis 2005]. The intermediate values lead to energetic variational estimates and to a symmetric indefinite system matrix. Figure 12 illuminates the effect of ω, plotted for two representative contrasts of the phase moduli and h_1/ℓ ratios.

In the first case, see Figure 12a, the choice of the reference media has almost negligible effect on the H–S solution error; the slight influence observed for the coarse discretization completely disappears upon cell refinement. This is not very surprising, as the homogenized solution depends on the first-order statistics only — recall (48) — and therefore can be retained by the discrete H–S method (up to controllable errors) for any choice of E^0. Results for the statically indeterminate structure, on the other hand, show a significant sensitivity to the value of ω. By a proper adjustment of the reference medium, the error can be reduced by an order of magnitude and can eventually reach the accuracy of extensive MC sampling. With increasing phase moduli contrast, however, the range of such ω values rapidly decreases; for $E_2/E_1 = 100$ one needs to satisfy $9 \cdot 10^{-4} \lesssim \omega \lesssim 1.5 \cdot 10^{-3}$ in order to recover the MC results. It is noteworthy that these values agree rather well with the particular choice of reference media used by Matouš [2003] when modeling composites with a high phase contrast using the methodology proposed by Dvorak and Srinivas [1999].

5.5. ***Influence of microstructure size.*** Finally, we investigate the influence of the microstructure size. Figure 13 summarizes the obtained results for a moderate phase contrast and the optimal setting of the H–S method identified in the previous sections. A similar conclusion can be reached for both case studies: for all three ℓ/L values, the H–S method is capable of reaching an accuracy of MC confidence intervals for the cell length h_1 approximately equal to half of the microscopic length scale ℓ. In other words, keeping the same number of DOFs as used to discretize the polarization problem, the accuracy of the method increases with the increasing ℓ/L ratio, which is exactly an opposite trend to that of the classical deterministic homogenization.

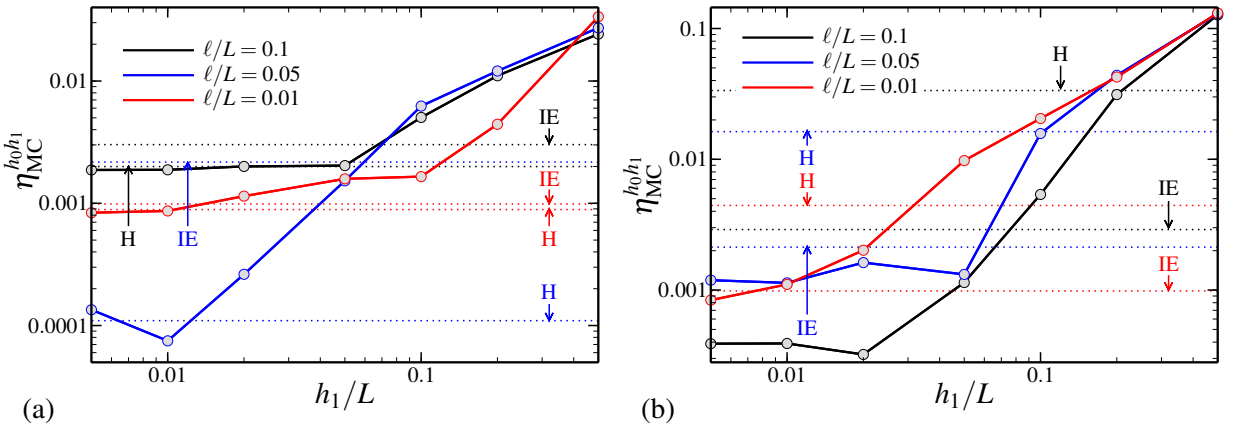

Figure 13. Influence of microstructure size: (a) statically determinate and (b) indeterminate structures; $E_2/E_1 = 5$, $\omega = 0.2$, $\ell/L = 0.05$, and $\mathbb{P}_0/\mathrm{GL}_2$ discretization.

6. Conclusions

In the present work, the predictive capacities of numerical methods based on the Hashin–Shtrikman–Willis variational principles, when applied to a specific model of functionally graded materials, have been systematically assessed. By restricting attention to the one-dimensional setting, an extensive parametric study has been executed and the results of numerical schemes have been verified against reliable large-scale Monte Carlo (MC) simulations. On the basis of the obtained data, we are justified in stating that:

- The Hashin–Shtrikman based numerical method, when set up properly, is capable of delivering results with accuracy comparable to detailed MC simulations and, consequently, of outperforming local averaging schemes.
- When applying the finite element method (FEM) to the solution of reference problem, the employed discretization has to be compatible with the numerics used to solve the polarization problem. If this condition is satisfied, the additional FEM-induced errors quickly become irrelevant.
- For the discretization of the reference problem, it appears to be advantageous to combine a low order (discontinuous) approximation of the polarization stresses with a higher order quadrature scheme to concisely capture the heterogeneity distribution.
- The correct choice of the reference medium has the potential to substantially decrease the error. Unfortunately, apart from [Dvorak and Srinivas 1999], we fail to give any a priori estimates of the optimal value for statistically nonhomogeneous structures.
- For accurate results, the characteristic cell size should be around 2–5 times smaller than the typical dimensions of the constituents.

The bottleneck in the current implementation is the solution of system (16), since it leads to a fully populated system matrix. Fortunately, as illustrated by Figure 14, the conditioning of the polarization problem seems to be dominated by the phase contrast rather than the discretization of the reference problem, which opens the way to efficient iterative techniques.

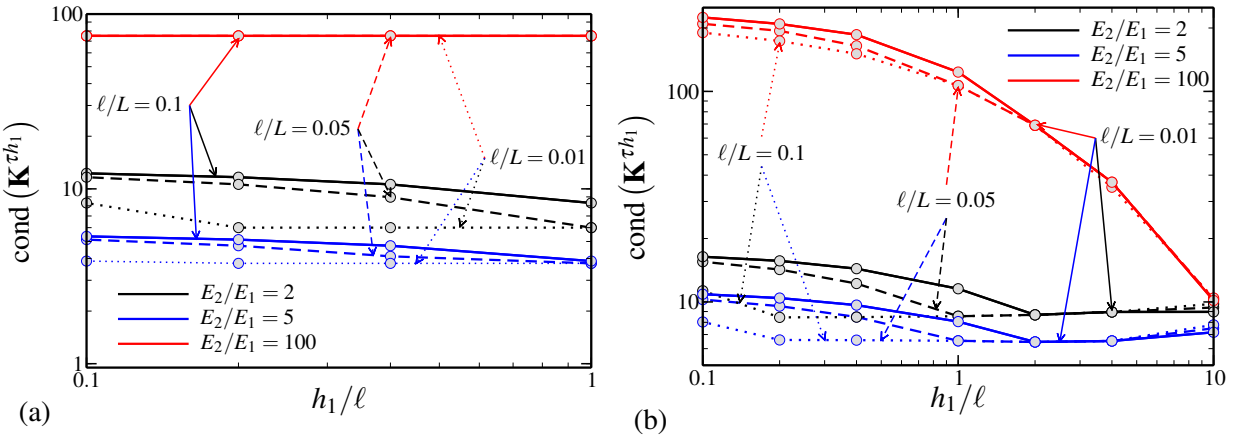

Figure 14. Sensitivity of conditioning of system matrix of the polarization problem: (a) statically determinate and (b) indeterminate structures; $\ell/L = 0.05$, $\omega = 0.2$, $\mathbb{P}_0/\mathrm{GL}_2$ scheme, and the condition number is estimated using the algorithm from [Higham and Tisseur 2000].

The next extension of the method would involve generalization to a multidimensional setting. For the FEM-based treatment, the key aspect remains a more rigorous analysis of the combined effect of the discretized Γ^0 operator, basis functions and integration scheme employed for the polarization problem. The multidimensional BEM approach, on the other hand, requires a careful treatment of the singularities of the Green's function-related quantities [Procházka and Šejnoha 2003] which are suppressed in the current one-dimensional setting. Such work will be reported separately in our future publications.

Acknowledgments

We would like to thank Jiří Šejnoha, Michal Šejnoha, Jan Novák and Milan Jirásek for numerous discussions on the topic of this work. The first author acknowledges the support from project No. 103/07/0304 (GA ČR). The work of the second author was supported by the research project MSM 6840770003 (MŠMT ČR).

Appendix: Overview of the simulation procedure

A crude MC method is employed to estimate the statistics of the local fields. In particular, given a number of simulations N_α, sampling points $0 = y_0 < y_1 < \ldots < y_{N_s} = L$, and an upper bound on the intensity $\rho^* \geq \sup_{x\in[0,L]} \rho(x)$, the following steps are repeated for $\alpha = 1, 2, \ldots, N_\alpha$:

Microstructure generation: Construction of a microstructural sample is based on a two-step procedure proposed for general Poisson processes in [Stoyan et al. 1987, Section 2.6]. First, the number of reference points $N_p^*(\alpha)$ is determined by simulating a Poisson random variable with mean $\rho^* L$. The coordinates of the reference points $z_1^*(\alpha), z_2^*(\alpha), \ldots, z_{N_p^*(\alpha)}^*(\alpha)$ then follow from a realization of $N_p^*(\alpha)$ independent random variables uniformly distributed on a closed interval $[0, L]$. Second, each point in the set is deleted with a probability $1 - \rho(z_p^*(\alpha))/\rho^*$, leading to a (relabeled) sequence of $N_p(\alpha)$ particle centers $z_p(\alpha)$.

Solution of the one-dimensional problem: With the microstructure realization fixed, the displacement of sampling points is computed by the recursion

$$u_{\mathrm{MC}}(y_s;\alpha) = u_{\mathrm{MC}}(y_{s-1};\alpha) + \int_{y_{s-1}}^{y_s} \frac{t(0;\alpha) - \int_0^x b(\xi)\,\mathrm{d}\xi}{E(x;\alpha)}\,\mathrm{d}x, \tag{A.1}$$

where the Young modulus is provided by (5) with the characteristic function χ_1 defined as

$$\chi_1(x;\alpha) = 1 \quad \Leftrightarrow \quad \min_{p=1,2,\ldots,N_p(\alpha)} \left|x - z_p(\alpha)\right| > \frac{\ell}{2},$$

and the boundary data $u(0;\alpha)$ and $t(0;\alpha)$ determined from a generalization of the system of boundary equations (32)–(33).

After completing the sampling phase, the first- and second-order local statistics are assessed using the unbiased values

$$\langle u\rangle_{\mathrm{MC}}(y_s) \approx \frac{1}{N_\alpha}\sum_{\alpha=1}^{N_\alpha} u_{\mathrm{MC}}(y_s;\alpha), \qquad \sigma^2_{\mathrm{MC}}(y_s) \approx \frac{1}{N_\alpha - 1}\sum_{\alpha=1}^{N_\alpha}\big(\langle u_{\mathrm{MC}}\rangle(y_s) - u_{\mathrm{MC}}(y_s;\alpha)\big)^2,$$

to arrive at the γ-confidence interval estimates [Rektorys 1994, Section 34.8]

$$\begin{aligned}\langle u\rangle(y_s) &\in \big[\langle u_-\rangle_{\mathrm{MC}}(y_s),\, \langle u_+\rangle_{\mathrm{MC}}(y_s)\big] \\ &= \left[\langle u\rangle_{\mathrm{MC}}(y_s) - t_{(1+\gamma)/2,N_\alpha-1}\frac{\sigma_{\mathrm{MC}}(y_s)}{\sqrt{N_\alpha}},\, \langle u\rangle_{\mathrm{MC}}(y_s) + t_{(1+\gamma)/2,N_\alpha-1}\frac{\sigma_{\mathrm{MC}}(y_s)}{\sqrt{N_\alpha}}\right],\end{aligned}$$

where $t_{\beta,n}$ denotes the inverse of the Student's t distribution function for value β and n DOFs.

The reference results reported in Section 5 correspond to the values obtained for $N_\alpha = 100{,}000$ simulations, confidence level $\gamma = 99.9\%$, 101 equidistant sampling points, and with the integral (A.1) evaluated with an adaptive Simpson quadrature [Gander and Gautschi 2000] with the relative tolerance set to 10^{-6}.

References

[Anné et al. 2006] G. Anné, S. Hecht-Mijic, H. Richter, O. van der Biest, and J. Vleugels, "Strength and residual stresses of functionally graded Al_2O_3/ZrO_2 discs prepared by electrophoretic deposition", *Scr. Mater.* **54**:12 (2006), 2053–2056.

[Bendsøe and Sigmund 2004] M. P. Bendsøe and O. Sigmund, *Topology optimization: theory, methods and applications*, 2nd ed., Springer, Berlin, 2004.

[Beran 1968] M. J. Beran, *Statistical continuum theories*, Monographs in Statistical Physics and Thermodynamics **9**, Interscience, New York, 1968.

[Bittnar and Šejnoha 1996] Z. Bittnar and J. Šejnoha, *Numerical methods in structural mechanics*, ASCE/Thomas Telford, New York/London, 1996.

[Böhm 2008] H. J. Böhm, "A short introduction to basic aspects of continuum micromechanics", ILSB Report 206, Institute of Lightweight Design and Structural Biomechanics, Vienna University of Technology, 2008, Available at http://www.ilsb.tuwien.ac.at/links/downloads/cdlfmdrep03.pdf.

[Buryachenko 2007] V. A. Buryachenko, *Micromechanics of heterogeneous materials*, Springer, New York, 2007.

[Buryachenko and Rammerstorfer 2001] V. A. Buryachenko and F. G. Rammerstorfer, "Local effective thermoelastic properties of graded random structure matrix composites", *Arch. Appl. Mech.* **71**:4–5 (2001), 249–272.

[Ching and Chen 2007] H. K. Ching and J. K. Chen, "Thermal stress analysis of functionally graded composites with temperature-dependent material properties", *J. Mech. Mater. Struct.* **2**:4 (2007), 633–653.

[Cho and Ha 2001] J. R. Cho and D. Y. Ha, "Averaging and finite-element discretization approaches in the numerical analysis of functionally graded materials", *Mater. Sci. Eng. A* **302**:2 (2001), 187–196.

[Duddeck 2002] F. M. E. Duddeck, *Fourier BEM: generalization of boundary element methods by Fourier transform*, Lecture Notes in Applied Mechanics **5**, Springer, Berlin, 2002.

[Dvorak and Srinivas 1999] G. J. Dvorak and M. V. Srinivas, "New estimates of overall properties of heterogeneous solids", *J. Mech. Phys. Solids* **47**:4 (1999), 899–920.

[Ferrante and Graham-Brady 2005] F. J. Ferrante and L. L. Graham-Brady, "Stochastic simulation of non-Gaussian/non-stationary properties in a functionally graded plate", *Comput. Methods Appl. Mech. Eng.* **194**:12–16 (2005), 1675–1692.

[Gander and Gautschi 2000] W. Gander and W. Gautschi, "Adaptive quadrature: revisited", *BIT* **40**:1 (2000), 84–101.

[Ghosh et al. 1995] S. Ghosh, K. Lee, and S. Moorthy, "Multiple scale analysis of heterogeneous elastic structures using homogenization theory and Voronoi cell finite element method", *Int. J. Solids Struct.* **32**:1 (1995), 27–62.

[Goupee and Vel 2006] A. J. Goupee and S. S. Vel, "Two-dimensional optimization of material composition of functionally graded materials using meshless analyses and a genetic algorithm", *Comput. Methods Appl. Mech. Eng.* **195**:44–47 (2006), 5926–5948.

[Grujicic and Zhang 1998] M. Grujicic and Y. Zhang, "Determination of effective elastic properties of functionally graded materials using Voronoi cell finite element method", *Mater. Sci. Eng. A* **251**:1–2 (1998), 64–76.

[Hashin and Shtrikman 1962] Z. Hashin and S. Shtrikman, "On some variational principles in anisotropic and nonhomogeneous elasticity", *J. Mech. Phys. Solids* **10**:4 (1962), 335–342.

[Higham and Tisseur 2000] N. J. Higham and F. Tisseur, "A block algorithm for matrix 1-norm estimation, with an application to 1-norm pseudospectra", *SIAM J. Matrix Anal. Appl.* **21**:4 (2000), 1185–1201.

[Kandula et al. 2005] S. S. V. Kandula, J. Abanto-Bueno, P. H. Geubelle, and J. Lambros, "Cohesive modeling of dynamic fracture in functionally graded materials", *Int. J. Fract.* **132**:3 (2005), 275–296.

[Krysl 2006] P. Krysl, *A pragmatic introduction to the Finite Element Method for thermal and stress analysis*, World Scientific, Singapore, 2006.

[Luciano and Willis 2001] R. Luciano and J. R. Willis, "Non-local constitutive response of a random laminate subjected to configuration-dependent body force", *J. Mech. Phys. Solids* **49**:2 (2001), 431–444.

[Luciano and Willis 2004] R. Luciano and J. R. Willis, "Non-local constitutive equations for functionally graded materials", *Mech. Mater.* **36**:12 (2004), 1195–1206.

[Luciano and Willis 2005] R. Luciano and J. R. Willis, "FE analysis of stress and strain fields in finite random composite bodies", *J. Mech. Phys. Solids* **53**:7 (2005), 1505–1522.

[Luciano and Willis 2006] R. Luciano and J. R. Willis, "Hashin–Shtrikman based FE analysis of the elastic behaviour of finite random composite bodies", *Int. J. Fract.* **137**:1–4 (2006), 261–273.

[Markworth et al. 1995] A. J. Markworth, K. S. Ramesh, and W. P. Parks, Jr., "Modeling studies applied to functionally graded materials", *J. Mater. Sci.* **30**:9 (1995), 2183–2193.

[Matouš 2003] K. Matouš, "Damage evolution in particulate composite materials", *Int. J. Solids Struct.* **40**:6 (2003), 1489–1503.

[Milton 2002] G. W. Milton, *The theory of composites*, Cambridge Monographs on Applied and Computational Mathematics **6**, Cambridge, Cambridge, 2002.

[Murat and Tartar 1997] F. Murat and L. Tartar, "Calculus of variations and homogenization", pp. 139–173 in *Topics in mathematic modelling of composite materials*, edited by A. Cherkaev and R. V. Kohn, Progress in Nonlinear Differential Equations and Their Applications **31**, Birkhäuser, Boston, 1997.

[Neubrand and Rodel 1997] A. Neubrand and J. Rodel, "Gradient materials: an overview of a novel concept", *Z. Metallkd.* **88**:5 (1997), 358–371.

[Noda 1999] N. Noda, "Thermal stresses in functionally graded materials", *J. Therm. Stresses* **22**:4–5 (1999), 477–512.

[Petrtýl et al. 1996] M. Petrtýl, J. Heřt, and P. Fiala, "Spatial organization of the haversian bone in man", *J. Biomech.* **29**:2 (1996), 161–167.

[Procházka and Šejnoha 2003] P. Procházka and J. Šejnoha, "A BEM formulation for homogenization of composites with randomly distributed fibers", *Eng. Anal. Bound. Elem.* **27**:2 (2003), 137–144.

[Procházka and Šejnoha 2004] P. Procházka and J. Šejnoha, "Extended Hashin–Shtrikman variational principles", *Appl. Math.* **49**:4 (2004), 357–372.

[Quintanilla and Torquato 1997] J. Quintanilla and S. Torquato, "Microstructure functions for a model of statistically inhomogeneous random media", *Phys. Rev. E* **55**:2 (1997), 1558–1565.

[Rahman and Chakraborty 2007] S. Rahman and A. Chakraborty, "A stochastic micromechanical model for elastic properties of functionally graded materials", *Mech. Mater.* **39**:6 (2007), 548–563.

[Ray et al. 2005] A. K. Ray, S. Mondal, S. K. Das, and P. Ramachandrarao, "Bamboo: a functionally graded composite-correlation between microstructure and mechanical strength", *J. Mater. Sci.* **40**:19 (2005), 5249–5253.

[Reiter and Dvorak 1998] T. Reiter and G. J. Dvorak, "Micromechanical models for graded composite materials, II: Thermomechanical loading", *J. Mech. Phys. Solids* **46**:9 (1998), 1655–1673.

[Reiter et al. 1997] T. Reiter, G. J. Dvorak, and V. Tvergaard, "Micromechanical models for graded composite materials", *J. Mech. Phys. Solids* **45**:8 (1997), 1281–1302.

[Rektorys 1994] K. Rektorys, *Survey of applicable mathematics*, vol. II, 2nd ed., Mathematics and its Applications **281**, Kluwer, Dordrecht, 1994.

[Santare and Lambros 2000] M. H. Santare and J. Lambros, "Use of graded finite elements to model the behavior of nonhomogeneous materials", *J. Appl. Mech.* (*ASME*) **67**:4 (2000), 819–822.

[Šejnoha and Zeman 2000] M. Šejnoha and J. Zeman, *Micromechanical analysis of random composites*, Habilitation thesis, Faculty of Civil Engineering, Czech Technical University in Prague, 2000, Available at http://mech.fsv.cvut.cz/~sejnom/download/hab.pdf.

[Sládek et al. 2005] V. Sládek, J. Sládek, and C. Zhang, "Domain element local integral equation method for potential problems in anisotropic and functionally graded materials", *Comput. Mech.* **37**:1 (2005), 78–85.

[Stoyan et al. 1987] D. Stoyan, W. S. Kendall, and J. Mecke, *Stochastic geometry and its applications*, Akademie-Verlag, Berlin, 1987.

[Sutradhar and Paulino 2004] A. Sutradhar and G. H. Paulino, "The simple boundary element method for transient heat conduction in functionally graded materials", *Comput. Methods Appl. Mech. Eng.* **193**:42–44 (2004), 4511–4539.

[Torquato 2001] S. Torquato, *Random heterogeneous materials: microstructure and macroscopic properties*, Springer, New York, 2001.

[Uemura 2003] S. Uemura, "The activities of FGM on new application", *Mater. Sci. Forum* **423–425** (2003), 1–10.

[Vemaganti and Deshmukh 2006] K. Vemaganti and P. Deshmukh, "An adaptive global-local approach to modeling functionally graded materials", *Comput. Methods Appl. Mech. Eng.* **195**:33–36 (2006), 4230–4243.

[Willis 1977] J. R. Willis, "Bounds and self-consistent estimates for the overall properties of anisotropic composites", *J. Mech. Phys. Solids* **25**:3 (1977), 185–202.

[Willis 1981] J. R. Willis, "Variational and related methods for the overall properties of composites", pp. 1–78 in *Advances in applied mechanics*, vol. 21, edited by C.-S. Yih, Academic Press, New York, 1981.

Received 26 Aug 2008. Revised 27 Oct 2008. Accepted 1 Nov 2008.

ZAHRA SHARIF-KHODAEI: zahra.sharif@gmail.com
Faculty of Civil Engineering, Department of Mechanics, Czech Technical University in Prague, Thakurova 7, Prague 6, 166 29, Czech Republic

and

Department of Aeronautics, Imperial College London, Prince Consort Road, London SW7 2AZ, Great Britain

JAN ZEMAN: zemanj@cml.fsv.cvut.cz
Faculty of Civil Engineering, Department of Mechanics, Czech Technical University in Prague, Thakurova 7, Prague 6, 166 29, Czech Republic
http://mech.fsv.cvut.cz/~zemanj